MAVEN Survey of Magnetic Flux Rope Properties in the Martian Ionosphere: Comparison with 3 Types of Formation Mechanisms

C. F. Bowers[1], J. A. Slavin[1], G. A. DiBraccio[2], G. Poh[2,3], T. Hara[4], S. Xu[4], D.A. Brain[5]

[1] Department of Climate and Space Sciences and Engineering, University of Michigan, Ann Arbor, Michigan, United States.

[2] Solar System Exploration Division, NASA Goddard Space Flight Center, Greenbelt, Maryland, USA.

[3] Center for Research and Exploration in Space Sciences and Technology II, Catholic University of America, Washington, D.C, USA.

[4] Space Sciences Laboratory, University of California, Berkeley, Berkeley, CA, USA.

[5] Laboratory for Atmospheric and Space Physics, University of Colorado, Boulder, CO, USA.

Key Points:

- Flux ropes form at Mars via three distinct processes: boundary wave instabilities, external reconnection, and internal reconnection.
- Across 1900 orbits, we identify and analyze 121 magnetic flux ropes within the ionosphere of Mars using observations from MAVEN.
- Using electron and magnetic field observations, we separate the flux ropes into three categories based on formation mechanism.

Abstract

Flux ropes are a magnetic field phenomenon characterized by a filament of twisted magnetic field with an axial core and outer helical wraps. They form in the Martian ionosphere via three distinct mechanisms: boundary wave instabilities (BWI), external reconnection (ER) between the interplanetary magnetic field and the crustal anomalies, and internal reconnection (IR) of the crustal anomalies themselves. We have identified 121 magnetic flux ropes from 1900 orbits using plasma and magnetic field measurements measured by the Mars Atmosphere and Volatile EvolutioN (MAVEN) spacecraft, and separate flux ropes into categories based on formation mechanism by analyzing electron signatures. We find evidence for flux ropes formed via BWI, ER, and IR mechanisms which comprise 9%, 34%, and 57% of our dataset, respectively. Flux ropes formed via different mechanisms exhibit differences in location and force-free radius, indicating the formation mechanism of a flux rope impacts their influence on the Martian plasma environment.

Plain Language Summary

Mars possess localized magnetic fields that are frozen into the crust of the planet and protrude out into space. On the dayside of Mars, the crustal fields interact with the charged particles and magnetic field lines that are emanating away from the Sun known as the solar wind. The processes involved in this interaction create the Martian "magnetosphere," and can have a variety of implications on the evolution of the Martian atmosphere. One biproduct of this interaction is a "magnetic flux rope," which is a twisted filament of magnetic flux and plasma. Flux ropes show evidence for the reconfiguration of magnetic field lines within the magnetosphere, and lead to atmospheric loss at Mars. Using data from the Mars Atmosphere and Volatile EvolutioN (MAVEN) spacecraft, we analyze 121 events in which the spacecraft encountered a flux rope along its orbit around Mars. This is the first study to show evidence for Martian flux ropes having been formed via three distinct formation mechanisms. Flux ropes formed via different mechanisms exhibit differences in geographic location and size, indicating the formation mechanism of a flux rope impacts their influence on the Martian magnetospheric and atmospheric environment.

1 Introduction

Magnetic flux ropes are a well-documented space plasma physics phenomenon that have been detected throughout the solar system, ranging from the lower solar corona (*Fillipov et al., 2015*)

to the magnetosphere of Saturn (*Jasinski et al., 2016*). An understanding of flux ropes and their formation mechanisms is important for research in all space plasma environments for two main reasons: 1) flux rope formation plays a fundamental role in the reconfiguration of magnetic topology and 2) flux ropes have physical effects on the ambient environment, which includes storing magnetic energy and acting as channels for charged-particle transport. The ubiquity of flux ropes throughout diverse plasma environments suggests various processes are responsible for their formation.

At intrinsic magnetospheres, such as Earth and Mercury, planetary flux ropes are frequently observed along the dayside magnetopause and believed to form via multiple X-line reconnection between the interplanetary magnetic field (IMF) and the global intrinsic planetary magnetic field (e.g., *Lee and Fu,* 1985, *Sun et al.,* 2016). Multiple X-line reconnection also occurs to form flux ropes in the cross-tail current sheet where magnetic fields are oppositely oriented in the two lobes (e.g., *Elphic et al.,* 1986, *Slavin et al.,* 2003, *DiBraccio et al.,* 2015). On the dayside of planets with intrinsic magnetic fields, a high shear between the dipole magnetic field and the IMF along the magnetopause may result in single X-line reconnection or multiple X-line reconnection, the latter forming at least two magnetic flux ropes. After their formation on the dayside of the planet, these flux ropes subsequently carry magnetic flux and plasma to the nightside of the planet.

Flux ropes have also been observed at Venus, Mars, and Titan where intrinsic planetary magnetic fields are absent (e.g., *Wolff et al.,* 1980, *Luhmann et al.,* 1985, *Cloutier et al.,* 1999, *Penz et al.,* 2004, *Martin et al.,* 2020). These flux ropes must form through different processes than those observed at magnetized planets with a global intrinsic magnetic field. For example, the IMF flux tubes penetrate into Venus' ionosphere and drape around the planet. The barrier between the fast moving tailward flows of the magnetosheath and the slower moving ionospheric plasma (i.e., the ionopause) is subject to the development of large amplitude boundary wave instabilities. Simulation results have suggested that boundary wave instabilities such as Kelvin-Helmholtz (KH) may become non-linear and lead to flux rope formation at the ionopause of Venus (e.g., *Terada et al.,* 2002, *Möstl et al.,* 2011). These flux ropes were observed to be small-scale structures (~10 km in radius) and are evidence for the twisting of draped IMF flux tubes in the ionosphere of Venus (*Luhmann et al.,* 1985).

Flux ropes in the Martian induced magnetosphere are of particular interest due to the localized magnetic anomalies preserved by the crust of the planet (*Acuña., et al.,* 1999). In the southern hemisphere, the crustal anomalies are strong (~100-1000 nT at the surface) and protrude into space creating "mini-magnetospheres" similar to the IMF-planetary interactions along the dayside magnetopause of magnetized planets. In the northern hemisphere, the crustal anomalies are much weaker, and do not inhibit the IMF flux tubes from penetrating deep into the ionosphere, creating a plasma environment similar to that at Venus. Together, these two hemispheres comprise a unique hybrid magnetosphere at Mars. Flux ropes play two major roles at Mars: 1) the rapid reconfiguration of planetary crustal magnetic fields and the acceleration of charged particles, and 2) atmospheric mass loss as planetary particles travel through their helical wraps and escape down the magnetotail.

Magnetic flux ropes have been observed in the ionosphere of Mars by the Mars Global Surveyor (MGS) (e.g., *Cloutier et al.*, 1999; *Vignes et al.*, 2004; *Briggs et al.*, 2011; *Hara et al.*, 2014) and the Mars Atmosphere and Volatile EvolutioN (MAVEN) spacecrafts (e.g., *Hara et al.,* 2017). The hybrid nature of Mars' magnetosphere suggests that these flux ropes may be created in processes similar to Venusian ionospheric flux ropes formed by KH instabilities, or perhaps by a process unique to the Martian plasma environment. *Brain et al.,* [2010] first reported the MGS observation of a flux rope forming as a result of crustal field detachment due to magnetic reconnection. Using the plasma analysis capabilities of MAVEN, *Hara et al.,* [2017] also provided a detailed analysis of a similar event and demonstrated that this single ionospheric flux rope contained multiple planetary ions including H^+, O^+, O_2^+, and likely CO_2^+.

There is evidence that flux ropes at Mars may form via at least of the following three distinct mechanisms:

1. The development of large-amplitude boundary wave instabilities (BWI), most probably KH, on the boundary between the fast tailward flows in the magnetosheath and the slowly moving ionospheric plasma, similar to those found on Venus. KH waves have been detected at Mars (*Ruhunusiri et al.,* 2016), and if these boundary waves steepen sufficiently, the IMF flux tubes frozen into the magnetosheath plasma may undergo magnetic reconnection and lead to flux rope formation as illustrated in Figure **1a**.
2. Multiple X-line external reconnection (ER) between the draped IMF and a crustal anomaly can form flux ropes in a manner similar to flux rope formation on the dayside

magnetopause of intrinsically magnetized planets (*Hara et al.*, 2014, *Hara et al.*, 2017), illustrated in Figure **1b**.

3. Single X-line internal reconnection (IR) of the crustal anomalies themselves (e.g., *Brain et al.*, 2010, *Beharrell et al.*, 2012, *Hara et al.*, 2014). As the solar wind plasma flows around Mars, the ram pressure may distort the crustal anomalies as they respond to maintain pressure balance, leading to single X-line reconnection between the field lines of the anomalies themselves resulting in flux rope formation illustrated in Figure **1c**.

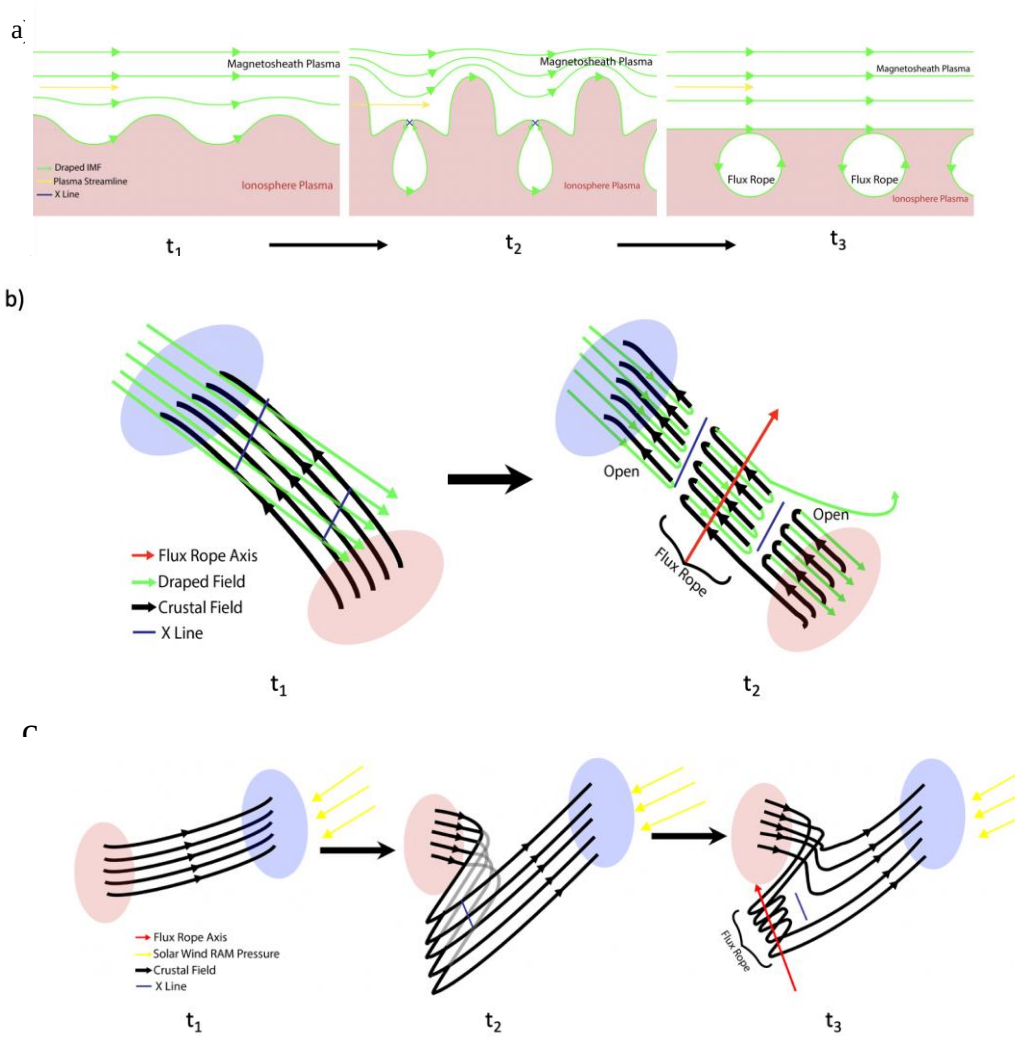

Figure **1**: *(a) Schematic demonstrating how a flux rope may form under the boundary wave instability mechanism, (b) external reconnection mechanism, and (c) internal reconnection mechanism. Red and blue ovals represent regions of crustal fields that point radially outward and inward, respectively. Black arrows represent crustal magnetic field lines, green arrows represent draped IMF field lines, yellow arrows represent flowing sheath plasma streamlines, blue lines or X's represent X-lines.*

Observations of flux ropes in the Martian ionosphere provide direct evidence for boundary wave instabilities or crustal field magnetic reconnection; however, there has been no comprehensive study of ionospheric flux ropes using the measurement capabilities of MAVEN to investigate their formation mechanisms. The work presented here conducts an extensive survey of flux ropes in the ionosphere of Mars. We use plasma data measured by MAVEN to estimate the magnetic topology of the flux ropes, providing evidence for three distinct formation mechanisms at Mars. Further analysis of the plasma contained within the flux ropes contributes to the fascinating topic of atmospheric mass loss at Mars.

2 Materials and Methods

2.1 Instrumentation

We investigate Martian flux ropes and their impact on the global magnetosphere and ionosphere through an analysis of data provided by the MAVEN spacecraft (*Jakosky et al.,* 2015). MAVEN's orbit precesses in both local time and longitude to provide global coverage of the Mars atmosphere and space environment with periapsis at ~150 km and apoapsis reaching ~6200 km. In particular, we analyze data provided by the Magnetometer (MAG) instrument (*Connerney et al.,* 2015) which measures vector magnetic fields at a maximum sampling rate of 32 vectors/s, the Solar Wind Electron Analyzer (SWEA) (*Mitchell et al.,* 2016), and the SupraThermal And Thermal Ion Composition (STATIC) instrument (*McFadden et al.,* 2015).

2.2 Methodology

Here, MAG data are analyzed in the Mars Solar Orbiter (MSO) and Minimum Variance Analysis (MVA) coordinate system. The MSO coordinate system is defined so that the X-axis points from the center of Mars towards the Sun, the Z-axis points towards geographic north, and the Y-axis completes the right-handed coordinate system. Magnetic flux rope signatures identified in the MAG data depend heavily on the orientation of the flux rope, as well as the spacecraft trajectory through the flux rope structure. In order to account for this variability, we transform the magnetic field data into MVA coordinates (*Sonnerup and Scheible*, 1998). In the MVA coordinate system for a flux rope, the N-direction defines the axis along which the magnetic field varies the least (i.e., minimum variance axis), and the N component (B_N) of the magnetic field remains steady throughout the extent of a flux rope. Note, the mean value of the B_N component of the magnetic

field is smallest for spacecraft trajectories that pass closest to the center of quasi-cylindrical flux ropes. The M-direction (intermediate variance) points orthogonal to the N-direction and along the central axis of quasi-force free flux ropes (*Slavin et al.*, 2003). B_M for a flux rope would therefore exhibit a unimodal peak corresponding to the axial field enhancement at the center of the flux rope. The L-direction (maximum variance) completes the right-handed coordinate system and points in the direction of the bipolar magnetic field (B_L) signature defined by the outer helical wraps. The full amplitude of this bi-polar B_L flux rope signature maximizes for spacecraft trajectories passing closest to the central axis of the flux rope.

We also analyze superthermal (>1eV) electron data from the SWEA instrument onboard MAVEN to estimate the source of the electrons that populate the flux rope and the surrounding plasma environment, as well as the magnetic topology. SWEA is capable of measuring electron fluxes at a 4 second cadence. We use these fluxes compared to the local magnetic field orientation and spacecraft location to parameterize the electron distribution as demonstrated by *Weber et al.*, 2017. This parameter is known as the pitch angle distribution (PAD) score and is defined by: (fFA- fperp)/σ , where fFA is the electron flux in the field aligned direction (the most field-aligned 10° available within pitch angles s 0-30° and 150-180°), fperp is the electron flux in perpendicular direction (pitch angles 85-95°), and σ is the propagated uncertainty. PAD score distinguishes among 3 electron distributions: (1) field-aligned beam distribution (PAD score >2), (2) isotropic distribution (- 3< PAD score <2), (3) loss cone distribution (PAD score <-3). We also compare the electron energy distribution to an expected distribution for photoelectrons at Mars to parameterize the likelihood that the measured electrons are composed of primarily photoelectrons or solar wind electrons (*Xu et al.*, 2017); this is known as the shape parameter. The shape parameter distinguishes between two electron populations: 1) photoelectrons (shape parameter < 1) and 2) solar wind electrons (shape parameter > 1). Both the PAD score and shape parameter are calculated for populations that are moving towards Mars and away from Mars by measuring the local inclination of the magnetic field and comparing it with the pitch angle distribution of the electrons. We compare all these parameters measured at a single time step to arrive at an estimation for the magnetic topology at the spacecraft's location (*Xu et al.*, 2019). The topology score can distinguish among 7 different topologies, which are numbered 1-7, with 0 indicating the data were insufficient to determine the topology.

MAVEN has a precessing elliptical orbit where the spacecraft samples throughout the magnetosphere and into the solar wind. This ensures that there are extended periods in which the spacecraft does not sample near dayside of Mars, where we assume most of the ionospheric flux ropes are formed. Therefore, we selected for orbits that sampled the low altitude (<1200 km) near-dayside (solar zenith angle (SZA) <110°) of the planet and visually inspected the MAG data for flux rope signatures.

3 Results

Throughout the 1900 orbits inspected, we identified 171 magnetic flux ropes. Of the 171 flux ropes identified, 156 show a sufficiently large (>2) max/intermediate eigenvalue ratio calculated from MVA. In MVA, the max/intermediate eigenvalue ratio is an indication of the accuracy of the coordinate definition. These flux ropes display a wide range in core field intensity (5-110 nT), and location in latitude (-75° - +75°) and longitude (1° - 358°). Of the 156 flux ropes selected, 140 contain sufficient electron data from SWEA to estimate magnetic topology. Below 160 km altitude, the superthermal electrons are dominated by local processes such as production and collisions which makes the topology score unreliable (*Xu et al.,* 2019). We therefore omit flux rope events that were detected below 160 km, leaving us with 121 events. The flux ropes that comprise our database exhibit three primary magnetic topologies (draped, open-dayside, closed-dayside). This variety in magnetic topology suggests that these flux ropes may have been formed via different formation mechanisms.

In order to categorize the formation mechanism of each flux rope, we examine the MAG, SWEA, and STATIC data that are available for each event. Depending on the signatures, a flux rope is assigned a formation mechanism of BWI, ER, or IR based on the following observations: if a flux rope were to form via the BWI mechanism, it would be populated primarily by electrons that have been traveling with the flow of the solar wind and the magnetic field lines would be connected on both ends to the IMF, which is classified as a draped magnetic field line. Thus, a draped topology score throughout a flux rope suggests that it had been formed via the BWI mechanism. If a flux rope were formed via the ER mechanism, the “opening up” of crustal magnetic field lines would allow solar wind plasma to mix with the ionospheric plasma that previously populated the closed magnetic loops of the crustal anomalies. Thus, flux ropes formed via the ER mechanism would contain both solar wind electrons and photoelectrons and exhibit open-dayside magnetic field topology. If a flux rope were to form via the IR mechanism, the flux

rope would be surrounded by closed magnetic topology and contain exclusively photoelectrons because the flux rope does not require any reconnection involving the IMF. Thus, flux ropes that exhibit closed-dayside magnetic topology throughout their structure are consistent with having been formed via the IR mechanism.

3.1 Case Studies

Figure **2** shows a time series of a flux rope signature in the MAVEN data. The flux rope can be identified by a characteristic increase in total magnetic field amplitude (Figure **2b**), and a unimodal peak in B_M coinciding with the inflection point of a bipolar signature in B_L (Figure **2c**). The shape parameter is >1 in both the away and towards directions throughout the flux rope signature (Figure **2e**), indicating that the flux rope is populated primarily by solar wind electrons

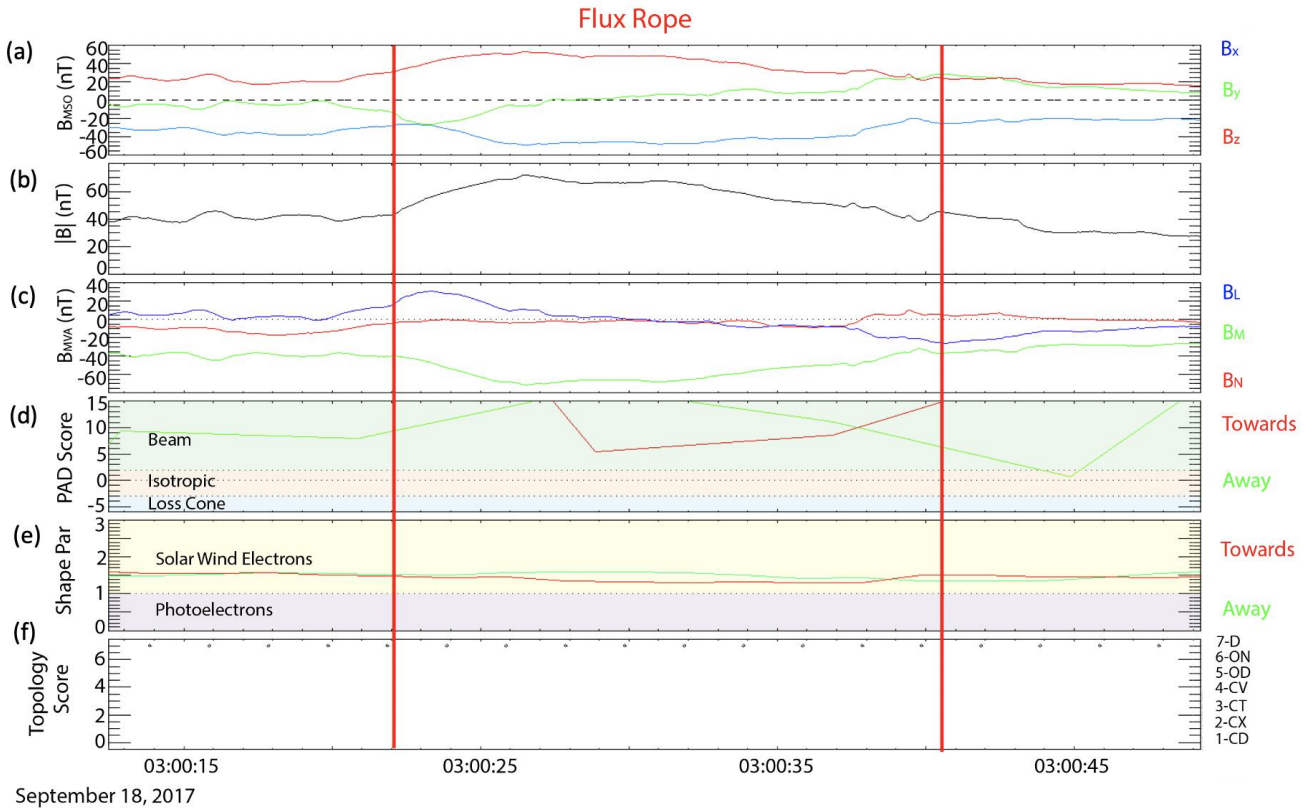

Figure **2**: *MAVEN observations of a flux rope detected on September 18, 2017, a) magnetic field in the MSO frame, b) magnetic field magnitude, c) magnetic field in MVA coordinate frame, d) PAD score, e) shape parameter, f) topology score*

rather than photoelectrons in both the away and towards direction. Therefore, the topology score throughout the flux rope is 7 (Figure **2f**), which indicates draped magnetic topology. Draped magnetic topology is expected if the flux rope were to have been formed via the BWI mechanism

illustrated in Figure **1a**. Of the 121 flux ropes in our database, 11 (9%) are consistent with hsaving been formed via the BWI formation mechanism.

Figure **3** shows a time series of a pair of flux ropes detected by MAVEN on May 14, 2018. From the onset of the first flux rope to ~18:52:30 the shape parameter is < 1 (Figure **3e**) and the topology score is = 1 (Figure **3f**), indicating the presence of photoelectrons and closed-dayside magnetic topology. For the remainder of the flux rope, the shape parameter in the towards direction remains >1, and the topology score is = 5, indicating the presence of solar wind electrons and open-dayside magnetic topology. Open-dayside magnetic topology is expected if the flux rope were to have been formed via the ER mechanism illustrated in Figure **1b**. 41 (34%) of flux ropes in our database are consistent with having been formed via the ER formation mechanism.

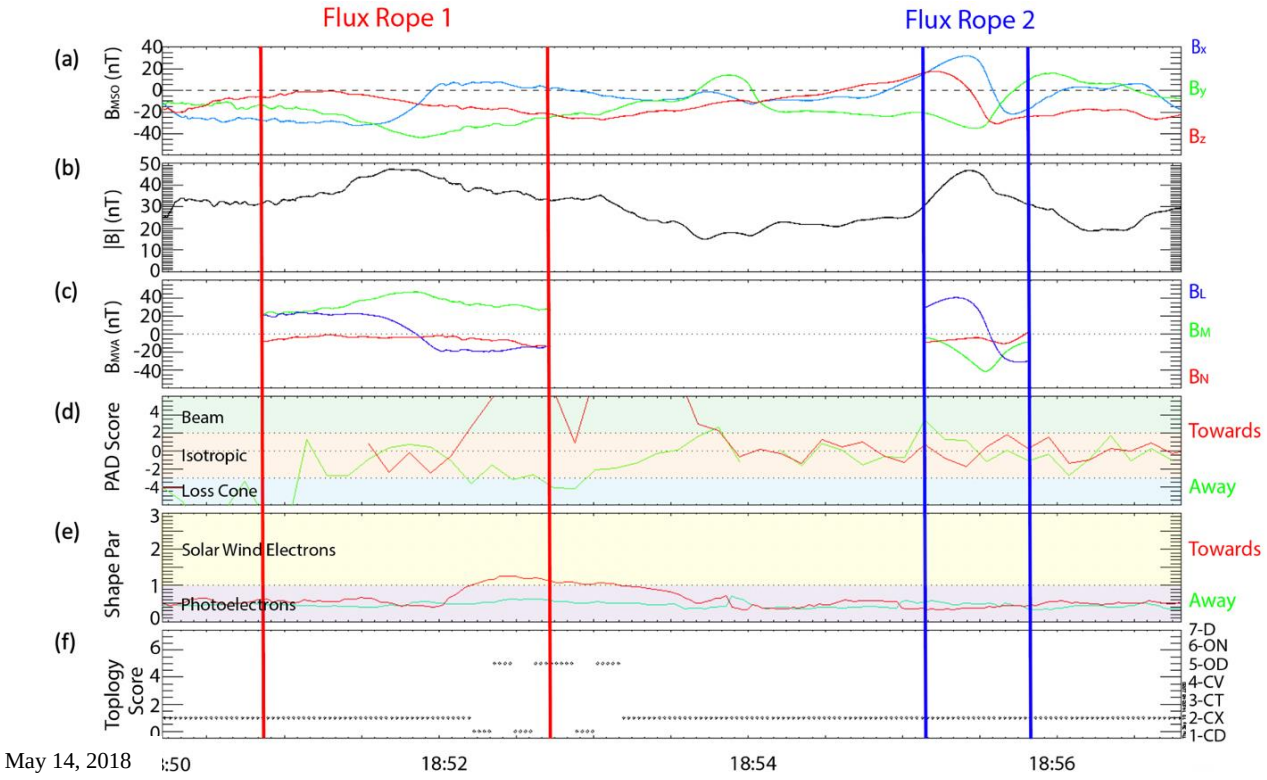

Figure **3**: MAVEN observations on May 14, 2018 in the same format as Figure **1**.

The second flux rope shown in Figure **3** maintains a shape parameter <1 and a topology score of 1 throughout the structure, indicating the presence of photoelectrons and closed-dayside magnetic topology, respectively. Closed-dayside topology is expected if the flux rope were to

have been formed via the IR mechanism illustrated in Figure **1c**. 69 (57%) of the flux ropes in our database are consistent with having been formed via the IR formation mechanism.

4 Discussion

Figure **4a** shows a histogram of altitudes at which flux ropes were detected, separated by formation mechanism. BWI flux ropes tend to occur at higher altitudes (median altitude = 670 km) than ER or IR flux ropes (median altitudes = 222 and 198 km, respectfully), which is consistent with the idea that BWI flux ropes form closer to the boundary between the magnetosheath and ionospheric plasma. Furthermore, Figure **4b** shows the occurrence rate of flux ropes measured by MAVEN in different latitude bins. BWI flux ropes tend to occur more frequently near the poles. This is consistent with BWI flux ropes forming as a result of velocity

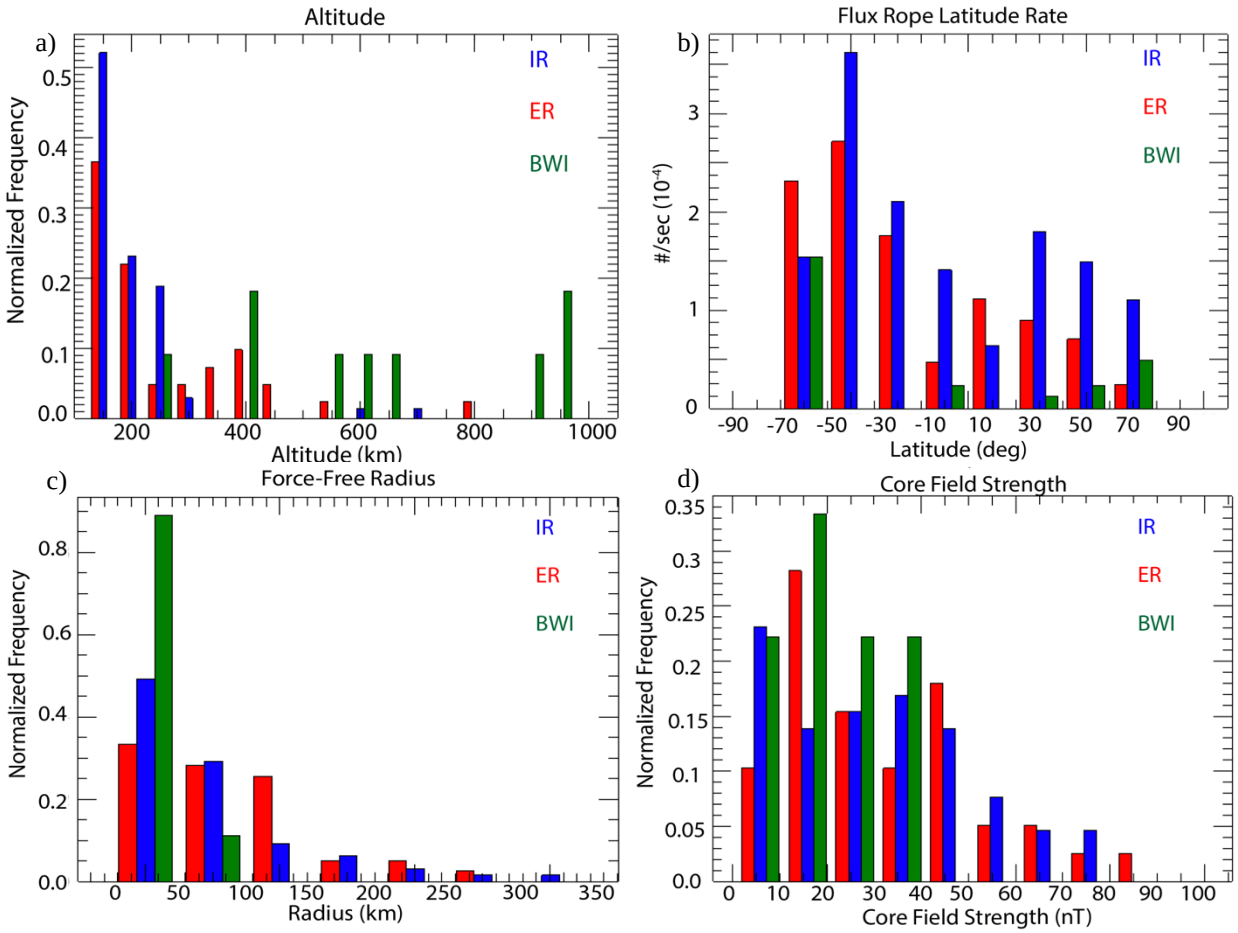

Figure **4**: *Flux rope properties separated by formation mechanism: a), Altitude at which the flux ropes were detected (km), b) flux rope occurrence rate at different latitudes (flux ropes/ second), c) flux rope radius estimated by the force-free model fit (km), d) Maximum field strength of the core field estimated by the force-free model (nT)*

shear because we expect the gradient between magnetosheath and ionospheric plasma to be greatest near the terminators. The ER and IR flux ropes occur most frequently in the mid-southern latitudes where the crustal magnetic fields are strongest, which is consistent with the notion that they were formed via reconnection between an anomaly and the IMF (ER), or reconnection of the crustal anomalies themselves (IR).

We implement a model in which flux ropes are assumed to be force-free ($\vec{J} \times \vec{B} = 0$) and stationary in order to estimate other properties of the flux ropes including radii and core-field strength at the center of the structure. Assuming cylindrical symmetry, *Lepping et al.,* 1996 showed that the axial and tangential magnetic field of a flux rope can be expressed with Bessel functions:

$$B_A = J_0(\alpha r')B_0, \qquad B_T = J_1(\alpha r')B_0 H\,, \qquad B_r = 0$$

B_A, B_T, B_R are the axial, tangential, and radial magnetic fields, $J_0(\alpha r')$, $J_1(\alpha r')$ are the zeroth- and first-order Bessel functions, B_0 is the magnetic field magnitude of the flux rope's core, and H is the handedness of the helicity. The parameter α is a constant at 2.4048 and represents the x-intercept of the zeroth-order Bessel function. The components of this modeled field thus depend on r', which is the radial distance from the center of the flux rope. We can apply this fitting technique to all 113 events in this study and implement a χ^2 test to select a radius that produces a best fit for each flux rope event. This best fit radius also allows us to estimate the absolute core-field strength of each event. Selecting for events where $\chi^2 < .02$, we find that 102 of the 121 flux ropes can be considered force-free. Of these 102 flux ropes, we see a great variety of radius estimates (2 km – 311 km) and core-field strength (6-110 nT). There is a strong linear correlation between impact parameter of the flux rope crossing determined by the force-free fitting and the normalized mean value of the N component of the magnetic field ($|B_N|/B_{max}$), where B_{max} is the maximum field strength within the flux rope (not shown). This correlation suggests that the MVA and force-free fitting analysis are in agreement.

We produce a histogram of radius and core-field strength separated by estimated flux rope formation mechanism (Figure **4c**, **4d**). Flux ropes formed through ER, IR have median radii of 64, 50 km, respectively. Flux ropes formed through BWI are the smallest of the three mechanisms, with a median radius of 5 km. This radius is in agreement with flux ropes found at Venus which have an estimated radius of ~10 km (*Luhmann et al.*,1985), further suggesting that

these flux ropes may have formed via a process similar to that at unmagnetized objects like Venus and Titan. Using data from the STATIC instrument, we are able to estimate the local gyroradius for three main species in the Martian ionosphere: H^+, O^+, and O_2^+ (median local gyroradii of 11 km, 74 km, and 113 km, respectively). If the radius of a flux rope is smaller than the gyroradius of a particle, then the particle cannot be frozen into the magnetic field of the flux rope, and the flux rope could not be a mechanism for ionospheric escape at Mars. Of the 102 flux ropes that are considered force-free, 77 (75%), 50(47%), and 41 (40%) have radii larger than the local gyroradius of H^+, O^+, and O_2^+ , respectively. This suggests that only a fraction of the flux ropes found in our database may contribute to the escape of planetary ions. While the efficiency of flux ropes ability to trap ionospheric H^+ does not depend on formation mechanism, no BWI flux ropes are large enough to trap O^+ or O_2^+ ions, suggesting BWI flux ropes are not an efficient mechanism for planetary ion escape. There is no significant difference between the IR and ER flux ropes in their ability to lead to ionospheric escape via plasma entrainment and propagation downstream. The core-field strength of the BWI, ER, and IR flux ropes does not vary greatly depending on formation mechanism (median values of 25 nT, 33 nT, 33 nT, respectively).

This is the first study that examines these three flux rope formation mechanisms using observations and statistics. The magnetosphere of Mars offers scientists a unique opportunity to study flux rope formation processes at a single object. This allows for fascinating comparisons among the properties of, and conditions that favor, flux rope formation at the planet. Our future work will investigate the dependency of flux rope formation on upstream solar wind conditions to better our understanding of the complex interaction between the solar wind and Martian plasma environments.

5 Summary

We visually inspected over 1900 orbits in which MAVEN sampled the dayside ionosphere of Mars. We transformed the MAG data into MVA coordinates to identify 156 magnetic flux ropes within the Martian ionosphere. Electron data from the SWEA instrument was used to determine magnetic topology of the flux ropes in order to estimate their formation mechanism. Each of the three magnetic topologies (draped, open-dayside, closed-dayside) that comprise the flux ropes within our database are consistent with a distinct formation mechanism: 1) boundary wave instabilities (BWI) like KH similar to flux ropes observed at Venus 2) external reconnection (ER) between the IMF and the crustal anomalies 3) internal reconnection (IR) of the crustal

anomalies themselves. The BWI flux ropes are the least common in our dataset, making up only 9% of the flux ropes, while the ER and the IR formation mechanisms make up 33% and 58% of the flux ropes, respectively. Using a force-free model fit, we were able to estimate the radii and core-field strength of the 129 flux ropes. The radii of flux ropes range from 2 km-360 km, and the core-field strength range from 5 nT-110 nT. Interestingly, the properties of BWI flux ropes including altitude at which they are detected, latitude, and median radius differ from the ER and IR flux ropes. Comparisons between the local gyroradii of planetary ions and the radii of the flux ropes suggests that roughly a third of the ER and IR flux ropes are large enough to trap heavy ions like O^+ and O_2^+, while no BWI flux ropes are sufficiently large to trap heavy ions.

Acknowledgments, Samples, and Data

The MAVEN project is supported by NASA through the Mars Exploration Program. MAVEN data are publicly available through the Planetary Plasma Interactions Node of the Planetary Data System (**https://pds-ppi.igpp.ucla.edu/mission/MAVEN**).

References

Acuña, M. H., et al. (1999), Global distribution of crustal magnetization discovered by the mars global surveyor MAG/ER experiment, Science, 284(5415), 790-793.

Beharrell, M., and J. Wild (2012), Stationary flux ropes at the southern terminator of Mars, Journal of Geophysical Research-Space Physics, 117(A12).

Brain, D., A. Baker, J. Briggs, J. Eastwood, J. Halekas, and T. Phan (2010), Episodic detachment of Martian crustal magnetic fields leading to bulk atmospheric plasma escape, Geophysical Research Letters, 37.

Briggs, J., D. Brain, M. Cartwright, J. Eastwood, and J. Halekas (2011), A statistical study of flux ropes in the Martian magnetosphere, Planetary and Space Science, 59(13), 1498-1505.

Cloutier, P., et al. (1999), Venus-like interaction of the solar wind with Mars, Geophysical Research Letters, 26(17), 2685-2688.

337 Connerney, J., J. Espley, P. Lawton, S. Murphy, J. Odom, R. Oliversen, and D. Sheppard (2015),
338 The MAVEN Magnetic Field Investigation, Space Science Reviews, 195(1-4), 257-291.
339 DiBraccio, G., et al. (2015), MESSENGER observations of flux ropes in Mercury's magnetotail,
340 Planetary and Space Science, 115, 77-89.
341
342 Elphic, R., C. Cattell, K. Takahashi, S. Bame, and C. Russell (1986), ISEE-1 and ISEE-2
343 Observations of Magnetic-Flux Ropes in the Magnetotail - FTES in the Plasma Sheet,
344 Geophysical Research Letters, 13(7), 648-651.
345
346 Filippov, B., O. Martsenyuk, A. Srivastava, and W. Uddin (2015), Solar Magnetic Flux Ropes,
347 Journal of Astrophysics and Astronomy, 36(1), 157-184.
348
349 Fu, Z., and L. Lee (1985), Simulation of Multiple X-Line Reconnection at the Dayside
350 Magnetopause, Geophysical Research Letters, 12(5), 291-294.
351
352 Hara, T., K. Seki, H. Hasegawa, D. Brain, K. Matsunaga, M. Saito, and D. Shiota (2014),
353 Formation processes of flux ropes downstream from Martian crustal magnetic fields inferred
354 from Grad-Shafranov reconstruction, Journal of Geophysical Research-Space Physics, 119(9),
355 7947–7962.
356
357 Hara, T., et al. (2017), MAVEN observations of a giant ionospheric flux rope near Mars resulting
358 from interaction between the crustal and interplanetary draped magnetic fields, Journal of
359 Geophysical Research-Space Physics, 122(1), 828-842.
360
361 Jakosky, B. M., M. Slipski, M. Benna, P. Mahaffy, M. Elrod, R. Yelle, S. Stone, and N. Alsaeed
362 (2017), Mars' atmospheric history derived from upper-atmosphere measurements of, Science,
363 355(6332), 1408-1410.
364 Jasinski, J., J. Slavin, C. Arridge, G. Poh, X. Jia, N. Sergis, A. Coates, G. Jones, and J. Waite
365 (2016), Flux transfer event observation at Saturn's dayside magnetopause by the Cassini
366 spacecraft, Geophysical Research Letters, 43(13), 6713-6723.
367

Lepping, R., J. Slavin, M. Hesse, J. Jones, and A. Szabo (1996), Analysis of magnetotail flux ropes with strong core fields: ISEE 3 observations, Journal of Geomagnetism and Geoelectricity, 48(5-6), 589-601.

Luhmann, J., and R. Elphic (1985), On the Dynamo Generation of Flux Ropes in the Venus Ionosphere, Journal of Geophysical Research-Space Physics, 90(NA12), 2047-2056.

Martin, C., C. Arridge, S. Badman, C. Russell, and H. Wei (2020), Distribution and Properties of Magnetic Flux Ropes in Titan's Ionosphere, Journal of Geophysical Research-Space Physics, 125(4), 1029-1043.

McFadden, J., et al. (2015), MAVEN SupraThermal and Thermal Ion Compostion (STATIC) Instrument, Space Science Reviews, 195(1-4), 199-256.

Mitchell, D., et al. (2016), The MAVEN Solar Wind Electron Analyzer, Space Science Reviews, 200(1-4), 495-528.

Möstl, U., N. Erkaev, M. Zellinger, H. Lammer, H. Groller, H. Biernat, and D. Korovinskiy (2011), The Kelvin-Helmholtz instability at Venus: What is the unstable boundary?, Icarus, 216(2), 476-484.

Penz, T., et al. (2004), Ion loss on Mars caused by the Kelvin-Helmholtz instability, Planetary and Space Science, 52(13), 1157-1167.

Ruhunusiri, S., et al. (2016), MAVEN observations of partially developed Kelvin-Helmholtz vortices at Mars, Geophysical Research Letters, 43(10), 4763-4773.

Slavin, J., R. Lepping, J. Gjerloev, D. Fairfield, M. Hesse, C. Owen, M. Moldwin, T. Nagai, A. Ieda, and T. Mukai (2003), Geotail observations of magnetic flux ropes in the plasma sheet, Journal of Geophysical Research-Space Physics, 108(A1), 1015-1033.

399 Sonnerup, B. U. Ö., and M. Scheible (1998), Minimum and maximum variance analysis, in
400 Analysis Methods for Multi-Spacecraft Data, ISSI Sci. Rep. no. SR-001, edited by G.
401 Paschmann and P. W. Daly, chap. 8, pp. 185–220, European Space Agency, Noordwijk,
402 Netherlands.
403
404 Sun, W., S. Fu, J. Slavin, J. Raines, Q. Zong, G. Poh, and T. Zurbuchen (2016), Spatial
405 distribution of Mercury's flux ropes and reconnection fronts: MESSENGER observations,
406 Journal of Geophysical Research-Space Physics, 121(8), 7590-7607.
407
408 Terada, N., S. Machida, and H. Shinagawa (2002), Global hybrid simulation of the Kelvin-
409 Helmholtz instability at the Venus ionopause, Journal of Geophysical Research-Space Physics,
410 107(A12), 1471.
411
412 Vignes, D., M. Acuna, J. Connerney, D. Crider, H. Reme, and C. Mazelle (2004), Magnetic flux
413 ropes in the Martian atmosphere: Global characteristics, Space Science Reviews, 111(1-2), 223-
414 231.
415
416 Weber, T., D. Brain, D. Mitchell, S. Xu, J. Connerney, and J. Halekas (2017), Characterization
417 of Low-Altitude Nightside Martian Magnetic Topology Using Electron Pitch Angle
418 Distributions, Journal of Geophysical Research-Space Physics, 122(10), 9777-9789.
419
420 Wolff, R. S., B. E. Goldstein, and C. M. Yeates (1980), The onset and development of Kelvin-
421 Helmholtz instabilities at the Venus ionopause, Journal of Geophysical Research: Space Physics,
422 85(A13), , 7697–7707.
423
424 Xu, S., T. Weber, D. Mitchell, D. Brain, C. Mazelle, G. DiBraccio, and J. Espley (2019), A
425 Technique to Infer Magnetic Topology at Mars and Its Application to the Terminator Region,
426 Journal of Geophysical Research-Space Physics, 124(3), 1823-1842.
427
428 Xu, S., et al. (2017), Martian low-altitude magnetic topology deduced from MAVEN/SWEA
429 observations, Journal of Geophysical Research-Space Physics, 122(2), 1831-1852.
430